Title

Modulating the behavior of ethyl cellulose-based oleogels: The impact food-grade amphiphilic small molecules on structural, mechanical, and rheological properties

Authors

Ji, Lei

Gravelle, Andrew J

Publication Date

2025-02-01

DOI

10.1016/j.foodhyd.2024.110703

Food Hydrocolloids 159 (2025) 110703

Contents lists available at ScienceDirect

Food Hydrocolloids

journal homepage: www.elsevier.com/locate/foodhyd

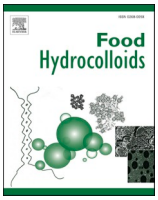

Modulating the behavior of ethyl cellulose-based oleogels: The impact food-grade amphiphilic small molecules on structural, mechanical, and rheological properties

Lei Ji, Andrew J. Gravelle *

Department of Food Science and Technology, University of California, Davis, USA

A B S T R A C T

This work evaluates the ability of various lipid-based amphiphilic small molecules (ASMs) to modulate the mechanical and rheological properties of oleogels principally structured by ethyl cellulose (EC). Six ASMs varying in the chemical structure of their polar headgroups were used to produce EC-ASM oleogels. Stearic acid (StAc), monoacylglycerol (MAG), sodium stearoyl lactylate (SSL), and citric acid esters of monoglycerides (CITREM) all provided a dramatic enhancement in gel strength, while lactic acid (LACTEM) and acetic acid (ACETEM) esters produced only a marginal increase. Those additives which crystallized above 20 °C displayed pronounced changes in their network organization and crystal morphology in the presence of EC. Differences in the solid/liquid phase change behavior were also observed in select samples using differential scanning calorimetry. Both the small and large amplitude oscillatory shear responses were dependent on the ASM which was dependent on the chemistry of the headgroup, crystal network organization, and ability to plasticize the polymer network. The extent of thixotropic recovery was largely dependent on the polarity of functional groups in the ASMs, but was also influenced by the formation of a secondary crystal network. In general, ASMs which formed larger, system-spanning crystal networks (MAG, StAc) produced more brittle gels, while the highly hydrophilic, charged headgroup of SSL promoted a homogeneous distribution of small crystals, resulting in a tougher material. In the absence of a crystal network, stronger polar species in the ASM headgroup produced higher gel strength and increased elasticity. Thus, both ASM chemical structure and crystallization properties strongly contribute to the functionality of the resulting combined oleogelator systems.

1. Introduction

Using structured edible oils in place of conventional fats from animals (e.g. lard, tallow, dairy fat) and tropical oils remains a consistent interest across the food industry (Pehlivanoğlu et al., 2018). While matching the functional traits of these products is an ongoing challenge among academic and industry researchers, considerable progress has been made in identifying strategies for producing structured oil systems which have expanded beyond simple lipid-based crystal-forming networks (Bascuas, Morell, Hernando, & Quiles, 2021; Sivakanthan, Fawzia, Madhujith, & Karim, 2022). These include multi-component crystalline networks, indirect structuring approaches developed to transform edible biopolymers into oil-structuring materials, and applying a variety of processing conditions, depending on the gelator of interest (Gravelle, Bovi Karatay, & Hubinger, 2024; Shakeel, Farooq, Gabriele, Marangoni, & Lupi, 2021; Vélez-Erazo, Okuro, Gallegos-Soto, da Cunha, & Hubinger, 2022). Some of these approaches include the formation of structural templates (foams or emulsions), use of heat-treatment, sonication, and solvent substitution, among others.

The type of gelator(s) and production method will not only impact the oleogel performance, but also impose constraints on the functional properties that can be achieved for a given oleogel system (Pinto, Sabet, Kazerani García, Kirjoranta, & Valoppi, 2024). For this reason, fundamental investigations exploring routes to expand or modulate the attributes of existing oleogelator systems remain an important area of further study (Sabet, Pinto, Kirjoranta, Garcia, & Valoppi, 2023). Among the various oil structuring strategies which have been explored for food applications, ethyl cellulose (EC) uniquely remains the only polymer which can form oleogels through a direct dispersion method (Gravelle, 2024). Commercial varieties of EC are produced with an ethoxyl content of ~48–49.5 wt%, leaving approximately one unsubstituted hydroxyl group for every two glucose monomers. When heated above its glass transition temperature (~130 °C), EC can be dispersed in triglyceride oils (Laredo, Barbut, & Marangoni, 2011). Upon cooling, the hydroxyl groups associate via hydrogen bonds, forming physical junction zones which support the entangled polymer network (Davidovich-Pinhas, Barbut, & Marangoni, 2015; Zetzl et al., 2014). Refined vegetable oils tend to be passively held within the EC network, resulting in a brittle structure and poor oil biding under mechanical stress (Gravelle, Barbut, Quinton, & Marangoni, 2014). However, it has been recognized that polar compounds present in the bulk oil phase or the addition of

* Corresponding author.
E-mail address: agravelle@ucdavis.edu (A.J. Gravelle).

https://doi.org/10.1016/j.foodhyd.2024.110703
Received 8 August 2024; Received in revised form 24 September 2024; Accepted 30 September 2024
Available online 2 October 2024

List of abbreviations

EC – ethyl cellulose
MAG – monoacylglycerol
StAc – stearic acid
SSL – sodium stearoyl lactylate
CITREM – citric acid esters of mono- and diglycerides
LACTEM – lactic acid esters of mono- and diglycerides
ACETEM – acetic acid esters of monoglycerides
DIC – differential interference contrast
LAOS – large amplitude oscillatory shear

amphiphilic compounds can dramatically influence the mechanical, rheological, and oil binding properties of these gels. A number of studies have shown that products of oil oxidation and chemical species present in unrefined oils including flaxseed, olive, and coconut oils can impact these attributes (Giacintucci et al., 2018; Gravelle, Davidovich-Pinhas, Zetzl, Barbut, & Marangoni, 2016; Silva et al., 2022). The addition of amphiphilic small molecules (ASMs) such as free fatty acids and food-grade surfactants have also been shown to modulate the performance of EC oleogels (Davidovich-Pinhas, Gravelle, Barbut, & Marangoni, 2015; Gravelle et al., 2014; Haj Eisa, Laufer, Rosen-Kligvasser, & Davidovich-Pinhas, 2020). Various ASMs are also known to be plasticizing agents for EC, and have been used to modulate its performance in films and barrier applications (Lin, Asante, et al., 2021; Lin, Li, et al., 2021; Shlush & Davidovich-Pinhas, 2023).

The addition of ASMs which are themselves oleogelators provides an opportunity to form cooperative multi-component systems which could be used to develop unique or tailored functional traits. EC has been used in combination with free fatty acids (Ahmadi, Tabibiazar, Roufegarinejad, & Babazadeh, 2020; Gravelle et al., 2016; Haj Eisa et al., 2020), fatty acid/fatty alcohol mixtures (Gravelle, Blach, Weiss, Barbut, & Marangoni, 2017; Gravelle, Davidovich-Pinhas, Barbut, & Marangoni, 2017), and plant-derived waxes (Rodríguez-Hernández, Pérez-Martínez, Gallegos-Infante, Toro-Vazquez, & Ornelas-Paz, 2021; Wang, Chandrapala, Truong, & Farahnaky, 2023; Zhang et al., 2024); however, the most commonly explored group of ASMs used in combination with EC has been monoglycerides (MAGs). García-Ortega et al. reported on the gelation properties of oleogels structured with EC and glycerol monostearate used near each of their critical gelation thresholds (García-Ortega, Alvarado, Martínez, & Vazquez, 2024). Others have explored the use of EC to prepare oleogel-in-water emulsions using an EC-MAG cooperative system (García-Ortega, Toro-Vazquez, & Ghosh, 2021; R. Zhang, Zhang, Yu, Gao, & Mao, 2022) and incorporate MAG into an EC-based oleogel as a means of modulating digestion behavior in a baked product (Chen, Lan, Li, Wang, & Wang, 2024). EC was also recently used to manipulate the functional properties of various vegetable oils which were subjected to enzymatic glycerolysis to generate MAGs and DAGs in situ (Soleimanian, Ghazani, & Marangoni, 2024a; Soleimanian, Ghazani, & Marangoni, 2024b). The selected oils had a wide range of unsaturated and saturated fatty acid composition and melting profiles, and the EC polymer network was intended to provide an additional structural element to mimic the properties of animal adipose tissue.

Due to the apparent interest in using ASMs to manipulate the properties of EC-based oleogels for food applications, the aim of this study was to systemically investigate how variations in the chemical structure of ASM headgroups affect the structural, mechanical, thermal, and rheological properties of canola oil-based EC oleogels. A total of five food-grade surfactants were evaluated: namely saturated monoglycerides (MAG), sodium stearoyl lactylate (SSL), and citric acid- (CITREM), lactic acid- (LACTEM), and acetic acid (ACETEM) esters of mono- or mono- and diglycerides. Finally, stearic acid (StAc) was investigated as a derivative of these ASMs, as it can be found as a naturally occurring component of unrefined oils, and it has been shown to have a dramatically influence on the mechanical properties of EC oleogels (Gravelle et al., 2016). A schematic illustration depicting representative structures of the selected ASMs is presented in Fig. 1.

2. Materials and methods

2.1. Materials

Canola oil was purchased from a local supermarket. EC (45 cP, 48–49.5% ethoxy content), stearic acid (StAc), and tert-butylhydroquinone (97%, TBHQ) were purchased from Sigma Aldrich (St. Louis, USA). Distilled monoacylglycerol (MAG; minimum 90% monoester content), sodium stearoyl lactylate (SSL), acetic acid esters of monoglycerides (ACETEM), lactic acid esters of mono- and diglycerides (LACTEM), citric acid esters of mono- and diglycerides (CITREM) were all kindly provided by International Flavors & Fragrances (IFF), Inc. (St. Louis, MO, USA). With the exception of CITREM, all ASMs were reported to be produced using hydrogenated vegetable oils. A summary of the sample nomenclature is provided in Table 1.

2.2. Sample preparation

EC oleogels were prepared based on a method described previously (Gravelle, Barbut, & Marangoni, 2012, 2016), with modifications. To minimize variability in sample preparation, stock batches of EC were prepared and divided before adding the small molecules. EC (8 wt%) was dispersed in canola oil by continuous stirring on a heating plate until reaching a temperature of ~150–160 °C. Once fully dispersed, the molten gel was cooled to room temperature overnight and split into 8

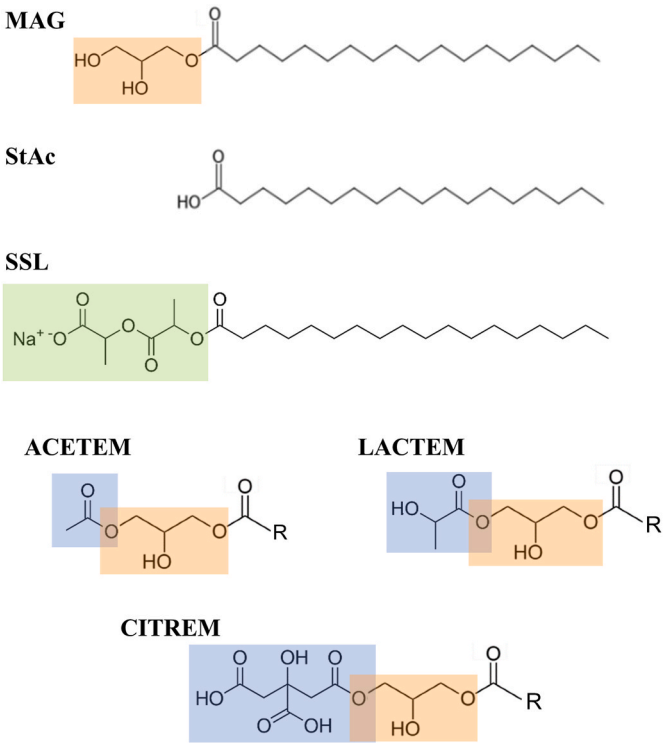

Fig. 1. Schematic illustration depicting representative chemical structures of the amphiphilic small molecules (ASMs) investigated: monoacylglycerol (MAG), stearic acid (StAc), sodium stearoyl lactylate (SSL), acetic acid esters of monoglycerides (ACETEM), lactic acid esters of mono- and diglycerides (LACTEM), and citric acid esters of mono- and diglycerides (CITREM). R denotes a fatty acyl chain (predominantly a saturated 18-carbon moiety).

Table 1
List of abbreviations for oil structuring compounds.

Abbreviation	Description
EC	Ethyl cellulose
ACETEM	Acetic acid esters of monoglycerides
LACTEM	Lactic acid esters of mono- and diglycerides
CITREM	Citric acid esters of mono- and diglycerides
SSL	Sodium stearoyl lactylate
StAc	Stearic acid
MAG	Monoglycerides (glycerol monostearate)

portions. The various surfactants were added (4 wt% relative to the oil phase) and each mixture was re-melted in a forced air convection oven (BINDER, Inc., New York, USA) held at 160 °C. The molten mixtures were thoroughly mixed, portioned, and gradually cooled to room temperature. Samples intended for large deformation analysis were split into 3 test tubes (height = 100 mm; diameter = 16 mm), while all other samples were kept in glass beakers until further use. 100 ppm of the antioxidant TBHQ was added to each sample prior to heating, and each sample was independently prepared in triplicate.

2.3. Microstructure

The crystal morphology was observed using an optical microscope (Olympus BX50 Olympus Corporation, Japan) using differential interference contrast (DIC) and polarized light modes. Prepared oleogels were portioned on a glass microscope slide (~5 mg), heated to ~160 °C, and a coverslip was applied while hot. Each slide was then cooled under ambient conditions and imaged within 24 h of preparation. Images were acquired using a digital camera (Industrial Digital Camera, Sony Exmor CMOS Sensor, Sony Group, Japan) and the Toupview software (ToupTek Photonics; Hangzhou, Zhejiang, China).

2.4. Large deformation mechanical analysis

The large deformation characteristics of EC-based oleogels were evaluated by back extrusion (Gravelle et al., 2012) using a TA.XTPlus texture analyzer equipped with a 5 kg load cell (Stable Micro Systems, Texture Technologies Corp., Scarsdale, NY). A stainless-steel probe with a cylindrical shaft (height 68 mm, diameter 8 mm) was used to penetrate 30 mm into each sample at a speed of 1 mm/s, and the resulting force response was recorded by the Exponent software. Each oleogel formulation (3 tubes per replicate) were performed in triplicate. A characteristic average back extrusion force-deformation profile of an oleogel is shown in Fig. 2*. The first peak where sample failure was observed was defined as the initial break force (F_b), while the gel firmness was defined as the average force from 15 to 30 mm penetration depth, which falls within the steady-state flow regime, as shown in Fig. 2 (Gravelle, Davidovich-Pinhas, et al., 2017).

2.5. Differential scanning calorimetry

The thermal behavior of EC-based oleogels (with and without surfactant) were evaluated using a differential scanning calorimeter (DSC 250, TA Instruments, New Castle, DE). The gels were weighed into a standard 40 μl aluminum pan and hermetically sealed with aluminum lid. The samples were analyzed using the following procedure: first heating from 20 °C to 100 °C, cooling from 100 °C to 0 °C, and second heating and cooling step from 0 °C to 80 °C and 80 °C–0 °C, respectively. Each heating/cooling step performed at a rate of 5 °C/min, with a 3 min isothermal equilibration phase between each step. The thermal transitions were characterized by the peak melting temperature (T_m), peak crystallization temperature (T_c), and total enthalpy of each heating and cooling step (ΔH_m and ΔH_c, respectively). Thermal analysis was performed using the TRIOS software package, v5 (TA Instruments).

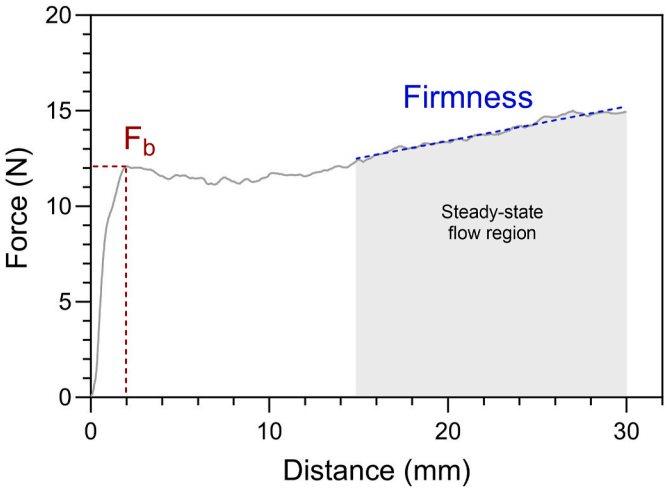

Fig. 2. Characteristic back extrusion force-deformation profile of an ethylcellulose-based oleogel. Physical parameters extracted from the plot are also labelled: F_b – break force; Firmness – average force during steady-state flow.

2.6. Rheological profiling

Rheological characterization was performed using an MCR302e rheometer (Anton Paar, Austria) equipped with a 25 mm sand-blasted base plate seated on a Peltier temperature control (P-PTD200/80/I) and a complementary 25 mm sand-blasted parallel plate geometry (PP25/S). For all measurements, prepared oleogels were melted on the pre-heated base plate (160 °C), followed by lowering the upper geometry (PP25/S) to a fixed gap size of 0.5 mm. Excess sample was trimmed, and the stage was cooled to 20 °C at a rate of 5 °C/min with fixed normal force of 1 N. Samples were allowed to equilibrate at 20 °C for 5 min prior to analysis. Unless otherwise stated, all experiments were performed at 20 °C. All measurements were performed at a fixed frequency of 1 Hz and were performed in triplicate.

2.6.1. Temperature sweep

Temperature sweep experiments were conducted using a strain of 0.1 %, which was determined to be within the linear viscoelastic (LVE) region of all samples. After loading the pre-made sample at 160 °C, measurements were performed as a cycle of cooling, heating and a second cooling using 5 °C/min cooling/heating rate, during which the storage modulus (G′) and loss modulus (G″) were recorded. Isothermal steps were performed for 2 min between cooling and heating phases.

2.6.2. Thixotropic behavior evaluation

Thixotropy measurement is crucial for assessing the strain recovery behavior of oleogels. Thixotropic behavior was evaluated using a five-stage oscillatory measurement using 0.1% and 100% strain alternating intervals, based on the method described previously (Haj Eisa et al., 2020). The first four stages were measured for 750 s, and the last stage was measured for 1500 s. The recovery was defined as the G′ at the end of stage five relative to the initial steady-state G′.

2.6.3. Large amplitude oscillatory shear (Laos)

To further evaluate the viscoelastic properties of samples at large deformations, the LAOS tests were performed based on a method described by Xia et al. (Xia, Siu, & Sagis, 2021) with slight modifications. After loading, the samples were subjected to a strain sweep from 1% to 1000% using a logarithmic strain ramp. G′ and G″ were recorded as a function of intercycle strain (γ_0), while shear stress (σ) was recorded as a function of intracycle strain (γ) and strain rate ($\dot{\gamma}$). Lissajous plots were constructed to analyze the non-linear rheological response of the

gels. The intracycle strain stiffening and intracycle shear thickening behaviors were quantified using the S-factor and a T-factor, respectively (Ewoldt, Hosoi, & McKinley, 2008):

$$S = \frac{G'_L - G'_M}{G'_L} \quad (1)$$

$$T = \frac{\eta'_L - \eta'_M}{\eta'_L} \quad (2)$$

Here, G'_L is the large-strain elastic modulus, also referred to as the secant modulus, G'_M is the shear elastic modulus at the minimum strain, also referred to as the tangent modulus at strain zero; η'_L is the viscosity at the maximum shear rate, and η'_M is the viscosity at the minimum shear rate.

2.7. Statistical analysis

Statistical analysis was conducted using SPSS 25.0 (IBM SPSS Inc. Chicago, IL, USA). One-way ANOVA (one-way analysis of variance) with Duncan's method ($p < 0.05$) were used to evaluate the statistical significance of differences among means. Lissajous plots were made with Python (version 3.2.2) other data figures were made using GraphPad Prism v10 (GraphPad Software, LLC).

3. Results and discussions

3.1. Microstructure

The microstructural properties of the EC-ASM oleogels which formed crystal networks at room temperature were evaluated by both DIC and polarized light (Fig. 3). While EC is known to form an entangled polymer network which physically entraps the liquid oil phase (Giacintucci et al., 2018; Zetzl et al., 2014), it is not observable by conventional light microscopy. Crystal structures were also not observed for either ACETEM or CITREM in either the presence and absence of EC and are thus also omitted.

The crystal morphology of the EC-based oleogels containing StAc, MAG, and SSL each produced crystalline structures which were homogeneously distributed throughout the gel network (Fig. 3A, C, 3E), but with highly distinct morphological features. In the EC-StAc oleogels (Fig. 3A) the StAc crystallites formed arching structures made of small, needle-like crystals with distinct gaps in the network where crystal formation was limited or absent. These features were particularly apparent in the DIC micrographs. This is in stark contrast to the larger,

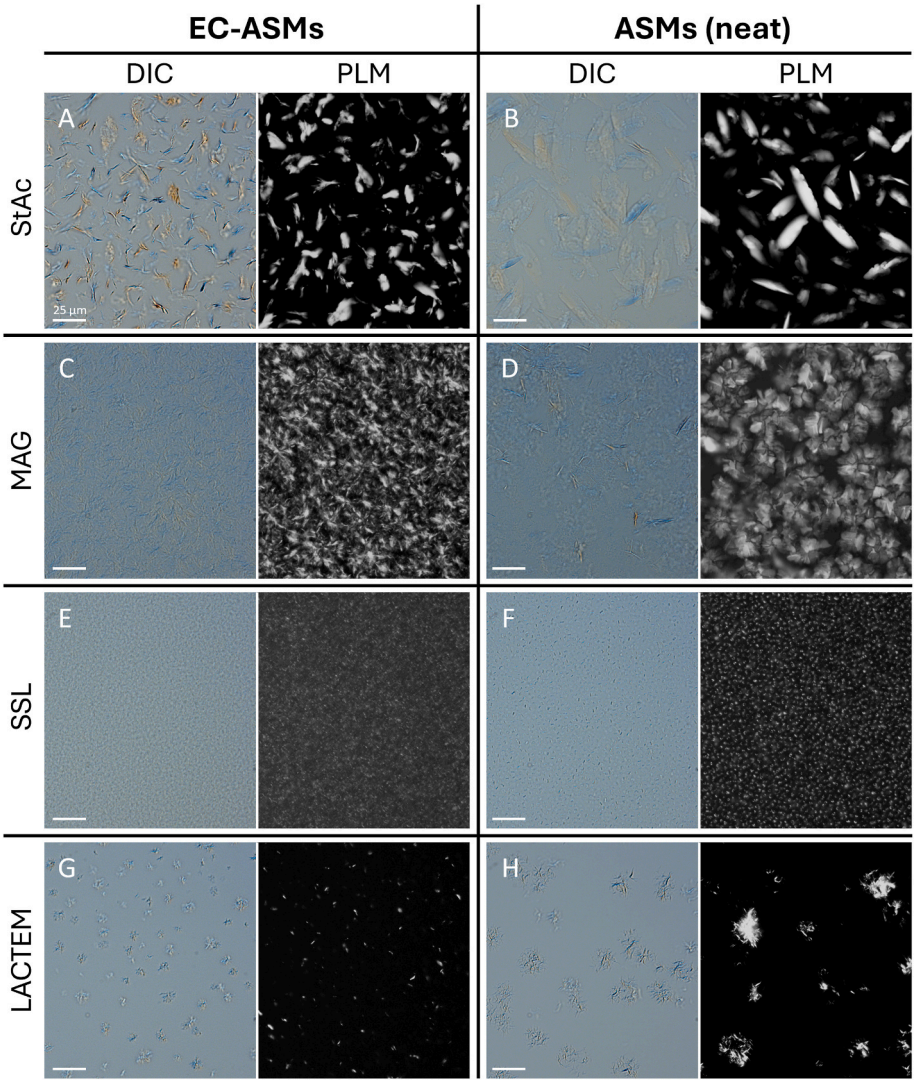

Fig. 3. Micrographs of EC-ASM hybrid oleogels imaged using differential interference contrast and polarized light microscopy (left and right of each panel, respectively). Oleogels were prepared with 8 wt% EC and 4 wt% ASM (A,C,E,G) or 4 wt% ASM alone (B,D,F,H). *For sample nomenclature, the reader is referred to Section 2.1.

randomly distributed platelets observed in the absence of EC (Fig. 3B) which have been shown to consist of tightly-packed, highly ordered lamellar structures supported by strong hydrogen bonding between the fatty acid headgroups (Rosen-Kligvasser & Davidovich-Pinhas, 2021). Although oleogels structured with higher concentrations of StAc (≥16 wt%) have been shown to form networks of branching platelets, this was proposed to result from crystal mismatch occurring during network formation, resulting in branching platelet-like structures (Sagiri, Singh, Pal, Banerjee, & Basak, 2015). The crystal morphology in the EC-StAc oleogel indicates the strong polarity of the carboxylic acid functional group of the free fatty acids causes them to preferentially associate with the EC polymer strands (Gravelle et al., 2016). This tendency has been attributed to polar interactions with the unsubstituted hydroxyl groups of EC, promoting the nucleation of crystallites along the polymer backbone which do not appear to extend into the bulk oil entrapped within the EC network (Gravelle, Blach, et al., 2017). The arching appearance is the result of the sample thickness and the 3-dimensional nature of these structures which pass through the focal plane. These morphological features are consistent with previous work on an oleogelator system combining EC with mixtures of stearyl alcohol and stearic acid at varying ratios (Gravelle, Blach, et al., 2017; Gravelle, Davidovich-Pinhas, et al., 2017).

In the EC-MAG oleogels (Fig. 3C), the MAG molecules appeared as a homogeneously dispersed network of spherulitic aggregates consisting of needle-like crystals radiating from distinct central points. In the absence of EC (Fig. 3D), the crystal network is less dense and appears as a collection of larger aggregated platelets. The difference in these networks indicates that MAG crystals in the EC-MAG gels also nucleate along the polymer backbone but form larger structures radiating out from these points which extend into the bulk oil. It has been shown that in contrast to StAc, the larger size and weaker polarity provided by the two free hydroxyl groups comprising the MAG headgroup (Fig. 1) form weaker hydrogen bonds, resulting in a looser lamellar packing arrangement in MAG-based oleogels (Rosen-Kligvasser & Davidovich-Pinhas, 2021). The lower polarity may also provide a higher solubility in the oil phase, promoting the formation of larger crystal aggregates in the EC-MAG system which extend through the bulk oil to form a space-filling network, and may further contribute to oil structuring.

The EC-SSL oleogels (Fig. 3E) produced a network of much smaller crystals which appeared as homogeneously dispersed discrete points. The hazy appearance in the polarized light micrograph is caused by the numerous crystals outside the focal plane. While a similar morphology can be observed in the absence of EC (Fig. 3F), these crystals are larger, and notably, these crystallites are simply dispersed in the oil, as the 4% SSL bulk mixtures sedimented over time. SSL-based oleogels have been previously reported using 7–13 wt% structurant; however, both the concentration and lactic acid content was shown to impact the crystal size, with a higher lactic acid content resulting in fewer and less aggregated crystals visibly by polarized light microscopy (Meng, Guo, Wang, & Liu, 2019). The SSL used in the present work was equivalent to the higher lactic acid variety used by Meng et al. (i.e., tending to form smaller crystals). The much smaller crystallites in the SSL samples can be attributed to the very strong hydrophilic properties of the carboxylic acid sodium salt (Fig. 1), which would strongly favor nucleation over crystal growth as the gel cools, resulting in the observed network of small, homogeneously dispersed crystals. The sodium salt would also provide a much stronger driving force to aggregate or associate with the hydroxyl groups along the EC backbone relative to the other ASMs investigated. The hydrophilic nature of the headgroup is also reflected in its relatively high HLB value (~8–10), and its limited solubility in oil (Du & Meng, 2023).

Finally, the EC-LACTEM oleogels produced randomly dispersed, isolated crystal aggregates with a needle-like morphology (Fig. 3G). In the absence of EC (Fig. 3H), there were fewer, and somewhat larger crystals, but with a similar overall appearance. Once again, the smaller crystallites formed in the presence of EC are expected to result from hydrophilic interactions between EC and the hydroxyl groups of LACTEM, promoting a greater degree of nucleation. However, an extensive crystal network was likely not formed due to the lower melting crystallization temperature of LACTEM (see Section 3.3). Thus, for all the ASMs which formed crystals at room temperature, EC tended to promote the formation of a greater number of smaller crystal aggregates, but the morphology of the resulting network was highly dependent on the chemical nature of each ASM headgroup.

3.2. Mechanical properties

To evaluate the effect of the various ASMs on the large-deformation mechanical behavior of EC oleogels, a back extrusion test was employed (Gravelle, Davidovich-Pinhas, et al., 2017). The force-deformation profiles (Fig. 4A) demonstrate that while all ASMs investigated increased the mechanical strength, the extent of reinforcement was dramatically dependent on the type of surfactant employed. Further, while a dependence of ASM type on gel strength has been reported by others (Davidovich-Pinhas, Gravelle, et al., 2015; Gravelle et al., 2014, 2016; Haj Eisa et al., 2020), only a select set of headgroups has been considered, and these have not been compared in the context of potentially cooperative oleogelator networks.

The additives which formed system-spanning crystalline networks within the EC gels produced the greatest extent of reinforcement (i.e., MAG, StAc, and SSL). The force-deformation profiles of the gels prepared with each of these additives were quite similar, despite the differences in crystal morphology and microstructural organization (Fig. 3). Notably, MAG and StAc displayed an abrupt increase up to a break point with little overshoot, followed by a gradual increase through the steady-state flow region (see Fig. 2 for terminology). Multicomponent oleogelator systems of EC prepared with both MAG (Davidovich-Pinhas, Gravelle, et al., 2015) and free fatty acids (Gravelle, Blach, et al., 2017; Haj Eisa et al., 2020) have each previously been shown to produce a synergistic enhancement in gel strength. This synergy is proposed to result from a combination of several factors: *i)* the hydrophilic interactions between EC and the ASM crystals directly strengthen the EC polymer network, *ii)* interactions between EC and the ASMs may enhance polymer plasticity and increase favorable interactions with the entrapped liquid oil, and *iii)* the ASM crystal network may also contribute to oil structuring. The latter is supported by the fact that unsaturated versions of the same ASMs also increase EC gel strength, but to a lesser extent. This has been explicitly reported for glycerol monostearate (equivalent to MAG used here) and its unsaturated counterpart, glycerol monooleate (Davidovich-Pinhas, Gravelle, et al., 2015). To further demonstrate the additional contribution of the crystal network, a comparison of F_b and gel firmness for EC-ASM oleogels prepared with either StAc or oleic acid is also provided as supplementary information (Fig. S1).

In contrast to MAG and StAc, the addition of SSL produced a lower break force (F_b), but a steeper rise in the force response over the remainder of the penetration test, resulting in a similar average gel strength though the steady-state flow regime. Of the additives which did not form system-spanning crystalline networks, CITREM imparted the greatest enhancement in gel strength. This can be attributed to the presence of the two carboxylic acid functional groups which would support hydrophilic interactions with EC, comparable to free fatty acids. The absence of the crystal network was due to the unsaturated nature of the fatty acid groups present in this product, which was produced from sunflower oil, while the other ASMs were produced from fully hydrogenated vegetable oils. However, CITREM was found to produce a similar increase in gel strength to oleic acid (see supplementary information, Fig. S1). This suggests that despite the larger headgroup of CITREM, the presence of two strongly polar carboxylic acid functional groups may result in a greater degree of interaction with EC, and possibly provide the opportunity for individual CITREM molecules to

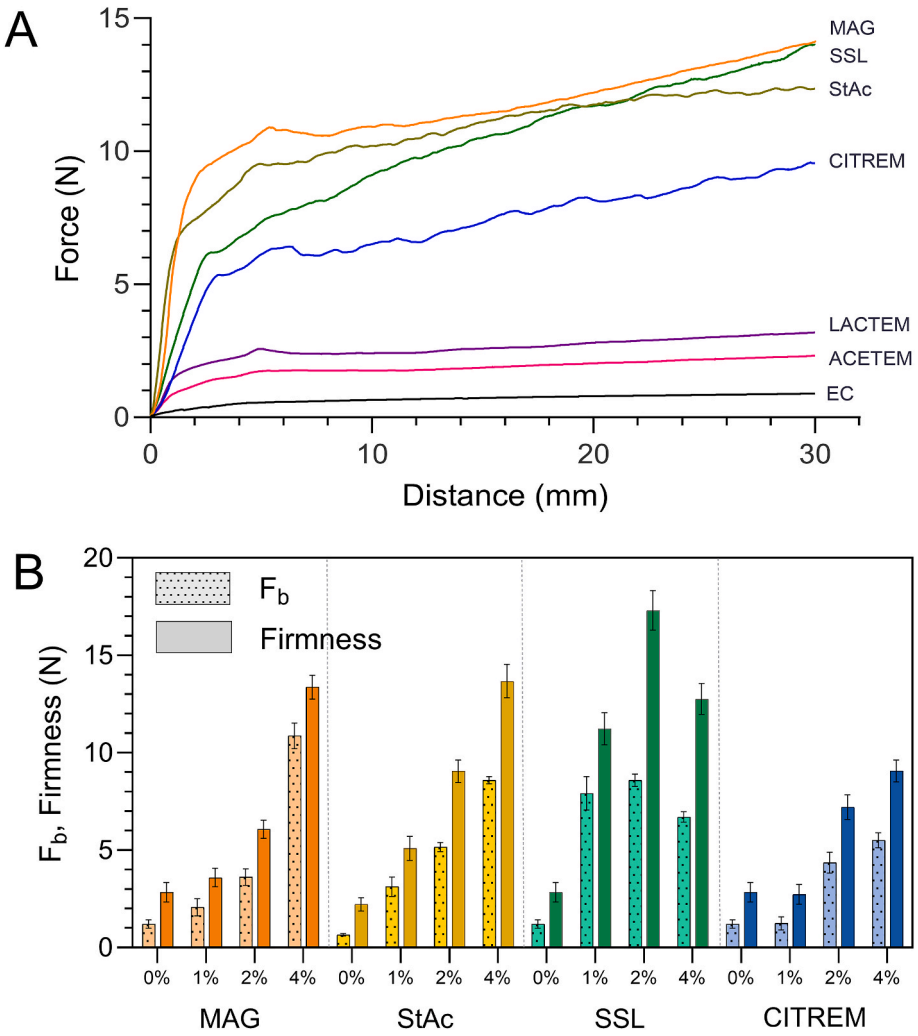

Fig. 4. Average back extrusion profiles for EC-based oleogels prepared with 4 wt% ASMs (A) and break force (F_b) and firmness values as a function of small molecule concentration for select additives (B). All oleogels were prepared with 8 wt% EC. *For sample nomenclature, the reader is referred to Section 2.1.

interact with multiple polymer strands.

While ACETEM and LACTEM also produced an increase in gel strength, their impact was relatively low compared to the other molecules evaluated. This can be attributed to the lower polarity of the functional groups of these additives, which have a substituent on the glycerol headgroup consisting of either a lone carbonyl (ACETEM) or a carbonyl and an adjacent hydroxyl group (LACTEM), as shown in Fig. 1. However, as LACTEM also formed dispersed crystals, further investigation would be required to confirm if the differences in gel strength of the EC-ACETEM and EC-LACTEM systems were exclusively caused by differences in their polar functional groups.

To gain additional insight into the impact of the small molecules on EC gel strength, the dose-response behavior of those gels which provided a >5-fold enhancement in firmness were also measured. Fig. 4B shows the F_b and firmness of oleogels prepared with increasing amounts of MAG, StAc, SSL, or CITREM. Both F_b and firmness followed a similar pattern, where firmness exceeded F_b due to the gradual rise in the force-deformation profile throughout the steady-state flow region. However, SSL produced a notably distinct behavior in which both parameters increased dramatically at low concentrations (1 wt%) but plateaued within the range of additive concentrations tested (2–4 wt%). This can again be correlated to the strongly hydrophilic nature of the sodium salt and the rapid formation of crystal nuclei which demonstrated a preference for forming much smaller crystals than the other ASMs evaluated. Further, the observed plateau at 2–4 wt% may be related to saturation of polymer-polymer junction zones with crystal nuclei and/or plasticization of the EC polymer. The latter has previously been observed at higher concentrations (5–10 wt%) for oleogels supplemented with oleic acid or oleyl alcohol, resulting in an analogous plateau in reinforcement (Gravelle et al., 2016). Thus, the much more hydrophilic nature of the SSL headgroup resulting from the charged carboxylate and sodium ions may provide an effective strategy to manipulate the strength of EC oleogels at lower concentrations.

3.3. Thermal behavior

The crystallization and melting profiles of the EC-ASM oleogels and 4 wt% ASMs mixtures in oil are presented in Fig. 5, and the associated thermal properties are provided in Table 2. EC is known to undergo a second-order glass transition at ~130 °C (Lai, Pitt, & Craig, 2010), which is required to fully disperse the polymer in vegetable oil and induce gelation (Davidovich-Pinhas, Barbut, & Marangoni, 2014; Gravelle, Davidovich-Pinhas, et al., 2017). Consistent with previous studies, no thermal event was observed for EC below this temperature, and only the first order thermal transitions of the small molecules are highlighted.

For ACETEM and CITREM, no crystallization or melting events were observed in the range of 10–100 °C, either in the presence or absence of EC. This is consistent with the microstructural observations and confirms no secondary crystalline network contributed to the structuring of

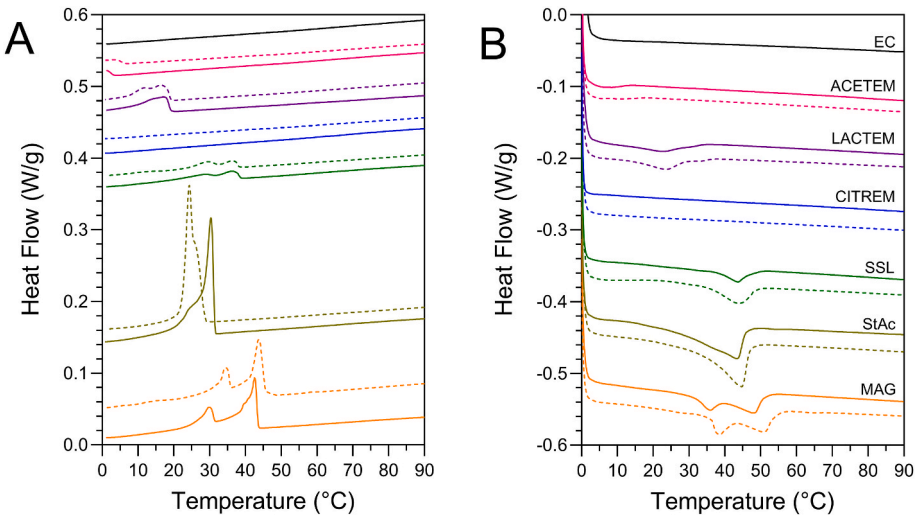

Fig. 5. Thermograms (Exo up) of oleogels prepared with 8% EC and 4% various ASMs (solid lines), or 4% ASMs alone (dashed lines) during melting (A) and crystallization (B). *For sample nomenclature, the reader is referred to Section 2.1.

Table 2
Melting and crystallization properties of oleogels prepared with 8% EC and 4% ASMs or 4% ASMs alone. ΔH and $T_{p,i}$ refer to the enthalpy and peak temperature of each thermal event. [a]For sample nomenclature, the reader is referred to Section 2.1.

Sample	Crystallization			Melting		
	ΔH_c (J/g)	$T_{c,1}$ (°C)	$T_{c,2}$ (°C)	ΔH_m (J/g)	$T_{m,1}$ (°C)	$T_{m,2}$ (°C)
EC	–	–	–	–	–	–
ACETEM	-[a]	-[a]	–	-[a]	-[a]	–
EC-ACETEM	-[a]	-[a]	–	-[a]	-[a]	–
LACTEM	2.18 ± 0.14	17.21 ± 1.10	12.69 ± 1.73	3.49 ± 0.15	23.30 ± 0.25	–
EC-LACTEM	1.92 ± 0.20	16.77 ± 0.67	13.62 ± 0.06	3.40 ± 0.01	22.39 ± 0.11	–
CITREM	–	–	–	–	–	–
EC-CITREM	–	–	–	–	–	–
SSL	1.53 ± 0.21	35.32 ± 1.54	28.64 ± 0.72	2.52 ± 0.23	43.71 ± 0.06	–
EC-SSL	1.65 ± 0.28	36.16 ± 0.47	27.35 ± 2.62	2.47 ± 0.12	44.03 ± 0.39	–
StAc	8.62 ± 0.27	25.50 ± 1.50	–	8.48 ± 0.38	44.56 ± 0.12	–
EC-StAc	7.55 ± 0.66	30.31 ± 0.20	21.47 ± 2.52	7.18 ± 0.32	43.3 ± 0.11	–
MAG	7.50 ± 0.15	43.63 ± 0.26	34.34 ± 0.23	7.92 ± 0.25	38.40 ± 0.28	51.09 ± 0.08
EC-MAG	6.54 ± 0.77	42.88 ± 0.67	29.50 ± 0.59	6.61 ± 0.71	36.04 ± 0.35	48.32 ± 0.36

[a] Crystallization/melting occurred below 10 °C, and thus not reported.

these oleogels. The remaining ASMs each displayed distinct thermal transition behavior, arising predominantly from the differences in the chemical structure of the headgroups. Notably, MAG and StAc had higher ΔH_c and ΔH_m than the other ASMs; however, these values decreased in the presence of EC (Table 2). The reduction in ΔH can be attributed to the interaction between the ASM polar headgroups and the EC backbone, which would reduce the interfacial free energy of crystal nuclei (Hondoh, Ueno, & Sato, 2018). This increases the chemical potential difference between the liquid and solid ASMs, resulting in a higher thermodynamic driving force for nucleation (Marangoni, 2017). The observed reduction in ΔH_c and ΔH_m in the presence of EC can therefore be correlated to the observed changes in crystal microstructure of MAG and StAc (Fig. 3). A similar decrease in ΔH_c has been reported when using MAG to structure triglyceride oils with hydrophilic functional groups in the oil phase, such as castor oil, which is rich in ricinoleic acid (Valoppi et al., 2017).

No notable differences in ΔH_c or ΔH_m were observed when SSL or LACTEM were crystallized in the presence or absence of EC. For SSL, this can be attributed to the high driving force for nucleation resulting from the unfavorable interactions between the ionic species in the headgroup and the liquid oil. Although EC influenced the number and distribution of SSL crystals, the unfavorable interactions with the hydrophobic solvent dominated the enthalpic contribution of these phase transitions. In contrast, the negligible impact of EC on the transition enthalpies of LACTEM can be attributed to the weaker interaction between the less polar functional groups of these molecules. This could also be observed in the minor changes in the crystal morphology of LACTEM when crystallized in the presence of EC.

Both the crystallization and melting profiles of MAG displayed two characteristic peaks (Fig. 5). The crystallization events have been attributed to the formation of a meta-stable inverse lamellar α-phase ($T_{c1} = 43.63 \pm 0.26$ °C) and reversible transition to the orthorhombic sub-α_1 phase ($T_{c2} = 34.34 \pm 0.23$ °C), respectively (Chen & Terentjev, 2009; Vereecken et al., 2009). The presence of the EC network caused a slight shift in the crystallization of the α-phase ($\Delta T_{c1} = -0.75$ °C), but notably also caused a greater depression in the α-to sub-α_1 polymorphic transition ($\Delta T_{c2} = -4.84$ °C). This suggests the interaction between EC and MAG provided additional stability to the α-phase, requiring a lower temperature to induce crystallization of the alkyl chains associated with the sub-α_1 form. There is also evidence of a minor third peak which forms at lower temperatures in the absence of EC and has been attributed to a second sub-α_2 polymorph (Vereecken et al., 2009). This peak is not apparent in the EC-MAG gel, suggesting the interaction with EC also stabilizes the higher-melting sub-α_1 form; however further investigation would be required to confirm this hypothesis.

Although a similar decrease in the α-phase crystallization temperature caused by EC has recently been reported (García-Ortega et al., 2024), the concentrations used were at or below the critical gelation

concentration (0.5–2 wt% MAG). As such, changes in the sub-α form were not be explored. These authors proposed the depression in crystallization temperature of the α-form ($T_{c,1}$) resulted from EC-MAG interactions depleting the concentration of free MAG in the liquid oil phase which is able to crystallize, thus effectively reducing the chemical potential for crystallization in oil. However, the microstructure of this oleogel (Fig. 3C) suggests such interactions promote the formation of nuclei which extend into the bulk oil phase. Thus, we proposed the overall shift in the phase transition behavior may be due to a combined effect of the hydrophilic interactions between EC and MAG and the relative solubility of MAG in triglyceride oils. The heating of the MAG and EC-MAG systems also show distinct melting peaks for the sub-α_1 and α-phases, which is consistent with previous reports on MAG-based oleogels (Li et al., 2021). The impact of EC-MAG crystal interactions were also apparent in the heating step, as the T_m of both the observed sub-α_1 and lamellar α-phases decreased by ~2–3 °C in the presence of EC.

In contrast to the impact on MAG, EC produced a marginal increase in the T_c of StAc, which is consistent with that observed in previous studies for oleogels consisting of 6 wt% EC and 5 wt% of a 3:7 mixture of StAc and stearyl alcohol in canola oil (Gravelle, Davidovich-Pinhas, et al., 2017). Interestingly, the opposite trend was observed for 10 wt % lauric acid oleogels prepared with increasing concentrations of 20 cP EC (0–8 wt%), also prepared in canola oil (Haj Eisa et al., 2020). This contradictory finding may be due to the higher concentration of free fatty acids used to structure the latter system, and the lower solubility of lauric acid in canola oil resulting from its shorter aliphatic chain relative to StAc. EC had little impact on T_c and T_m for either SSL or LACTEM, which is consistent with the observed impact on microstructure. Thus, the presence of EC predominantly impacted the crystallization and melting behavior of MAG and StAc, which can be associated with the formation of lamellar structures and a supporting crystal network, as outlined in Section 3.1.

3.4. Rheological behavior

3.4.1. Strain sweep

A characteristic strain sweep plot for the oleogel structured with EC alone is presented in Fig. 6A. This figure demonstrates the 4 characteristic regions commonly observed as soft materials transition from linear to non-linear viscoelastic behavior (John, Ray, Aswal, Deshpande, & Varughese, 2019); (1) the elastic-dominated LVE region, (2) onset of non-linearity, (3) cross-over of G′ and G″, and (4) the viscous-dominated regime. The behavior observed in Fig. 6A falls into the Type I classification of complex fluids described by Hyun et al. (Hyun, Kim, Ahn, & Lee, 2002), which exhibit strain thinning in both G′ and G″, and no evidence of a strain overshoot in either modulus. This type of viscoelastic response in polymeric systems is analogous to strain thinning behavior resulting from alignment of polymer chains or microstructures with the applied shear field (Hyun et al., 2002). In the case of EC oleogels, this response can be attributed to the physical nature of EC polymer network which is supported by intermolecular hydrogen bonds between the unsubstituted hydroxyl groups on the polymer backbone (Davidovich-Pinhas et al., 2015; Laredo et al., 2011). The relatively weak and brittle nature of these junction zones causes irreversible breakage and eventual failure of the gel with increasing strain.

The strain sweep plots for the EC-ASM oleogels are presented in Fig. 6B and C. The majority of the ASM additives maintained the Type I response, and predominantly impacted the LVE strain range. Interestingly, only the EC-MAG oleogel displayed a mild strain overshoot in G″, or Type III behavior (Hyun et al., 2002). This could be attributed to fluctuations in inter-crystal distances of the MAG network while responding to the applied deformation. However, this effect was not observed for either StAc or SSL, which also formed system-spanning crystal networks. This difference may be due to the distinct morphological features of the crystals in EC-MAG, which formed a homogeneous

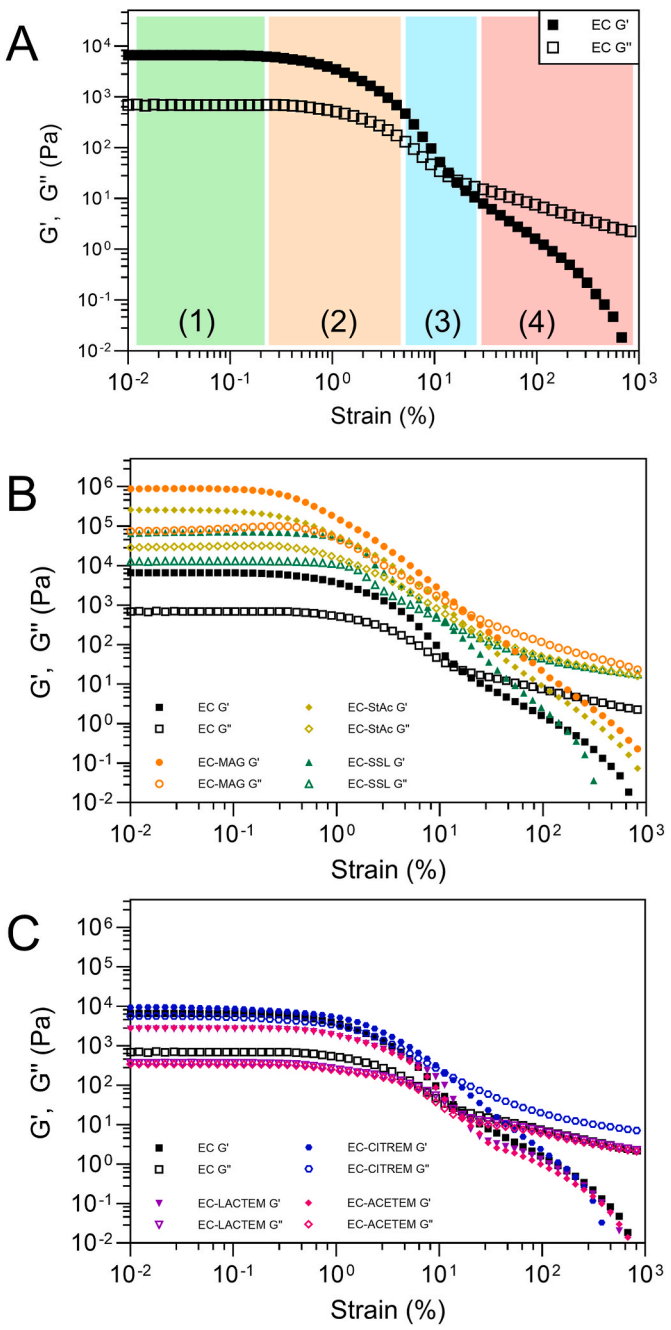

Fig. 6. Elastic (G′) and viscous (G″) shear moduli as a function of strain amplitude for oleogels prepared with 8% EC and 4% various ASMs. Panel (A) depicts a representative strain response for oleogels structured with EC alone, with numbered regions highlighting distinct viscoelastic behavior is observed in the Lissajous plots; Panels (B) and (C) depict strain response of the EC-ASM hybrids. *For sample nomenclature, the reader is referred to Section 2.1.

network of spherulitic aggregates throughout the oil phase, while EC-StAc and EC-SSL formed distinct structures along the polymer backbone. The weaker hydrogen bonding and less ordered lamellar structures reported for MAG oleogels (Rosen-Kligvasser & Davidovich-Pinhas, 2021) could allow the crystal network to resist deformation up to a critical strain, resulting in the observed overshoot.

Additional yielding and flow parameters extracted from the strain sweep measurements are summarized in Table 3. It is worth noting that compared to EC alone, only the EC-MAG and EC-StAc oleogels produced a decrease in the yield strain (σ_o). Free fatty acids in particular are well-known plasticizers of EC, and this plasticizing effect has been previously

Table 3
Yielding and flow parameters of EC-ASM oleogels. Yield point and flow point were defined as 5% deviation from linearity and G' = G″, respectively. *For sample nomenclature, the reader is referred to Section 2.1.

Gelator system	Yield strain (%)	Yield stress (Pa)	Flow strain (%)	Flow stress (Pa)
EC	0.29	14.2	16.0	5.2
EC-ACETEM	0.34	9.2	17.0	3.5
EC-LACTEM	0.34	8.7	17.0	4.0
EC-CITREM	0.89	51.1	11.0	34.0
EC-SSL	0.61	380.2	11.3	59.1
EC-StAc	0.11	246.3	16.5	79.5
EC-MAG	0.11	892.8	16.5	173.9

demonstrated in EC oleogels incorporating both StAc (Gravelle et al., 2016) and lauric acid (Haj Eisa et al., 2020). However, the formation of the polymer-crystalline network also results in stiffer gels (higher G′ and G″) at low strain amplitude, contributing to the observed decrease in the σ_o. Interestingly, the flow strain of EC-ASM oleogels was nearly unchanged relative to those structured with EC alone, indicating the lower σ_o can be attributed to a stiffening of the polymer network due to the association with the ASM crystallites.

It was observed that both the EC-SSL and EC-CITREM oleogels showed a relatively higher σ_o (0.61 and 0.89%, respectively) but lower flow strain (~11%), corresponding to a shorter Region 2 strain range (Fig. 6A). This indicates these ASMs produce a hybrid network which has a greater resilience (flexibility) and can withstand a higher degree of deformation before yielding; however, they also display a shorter solid-like phase, and exhibit flow at comparatively lower strain values, resulting in a narrow strain range where they exhibit plastic deformation. As no crystal network formed in the EC-CITREM oleogels, it appears that the addition of CITREM assists in creating a more elastic network, prone to deformation with a larger LVE region, resulting in the formation of a more rubbery (i.e., firm, but elastic) material. In contrast, the discrete network of SSL crystallites locally reinforce the polymer network, but also lead to failure under higher strain. These findings align with the large-deformation mechanical properties analysis (Fig. 4), as it was observed both these gels have lower Fb values than EC-MAG and EC-StAc. The EC-CITREM gels were also found to have a more elastic consistence with minimal oil leakage upon deformation, while the EC-SSL gels released more oil when fractured.

3.4.2. Temperature sweep

The cross-over temperature (where G' = G″) provides an indication of the thermally induced sol/gel transition point. The cross-over temperatures for the EC and EC-ASM oleogels for both the heating and cooling phases and associated thermal profiles for the cooling phase are presented in Fig. 7.

With the exception of EC-CITREM, the cross-over temperature was higher during the heating stage (melting) compared to the cooling stage (gelation) for both EC and EC-ASM oleogels. This is consistent with previous studies on the melting and gelation behavior of EC oleogels of varying molecular weight (Davidovich-Pinhas, Barbut, & Marangoni, 2015). For CITREM, G′ remained greater than G″ at all tested temperatures, indicating this system retained its solid-like behavior throughout the entire heating process. This behavior indicates the carboxylic acid functional groups of CITREM form direct, strong hydrogen-bonding interactions with the hydroxyl groups of EC. Further, the presence of multiple functional groups may allow individual CITREM molecules to interact with hydroxyl groups on adjacent polymer strands. In contrast to StAc molecules which tend to form stable dimers, the multiple polar functional groups of CITREM would make it difficult to form stable intramolecular interactions, thus leaving polar groups exposed and available to interact with EC, even at elevated temperatures.

Compared to the gels structured with EC alone, the addition of MAG, StAc, and SSL each decreased the gelation and melting temperature of

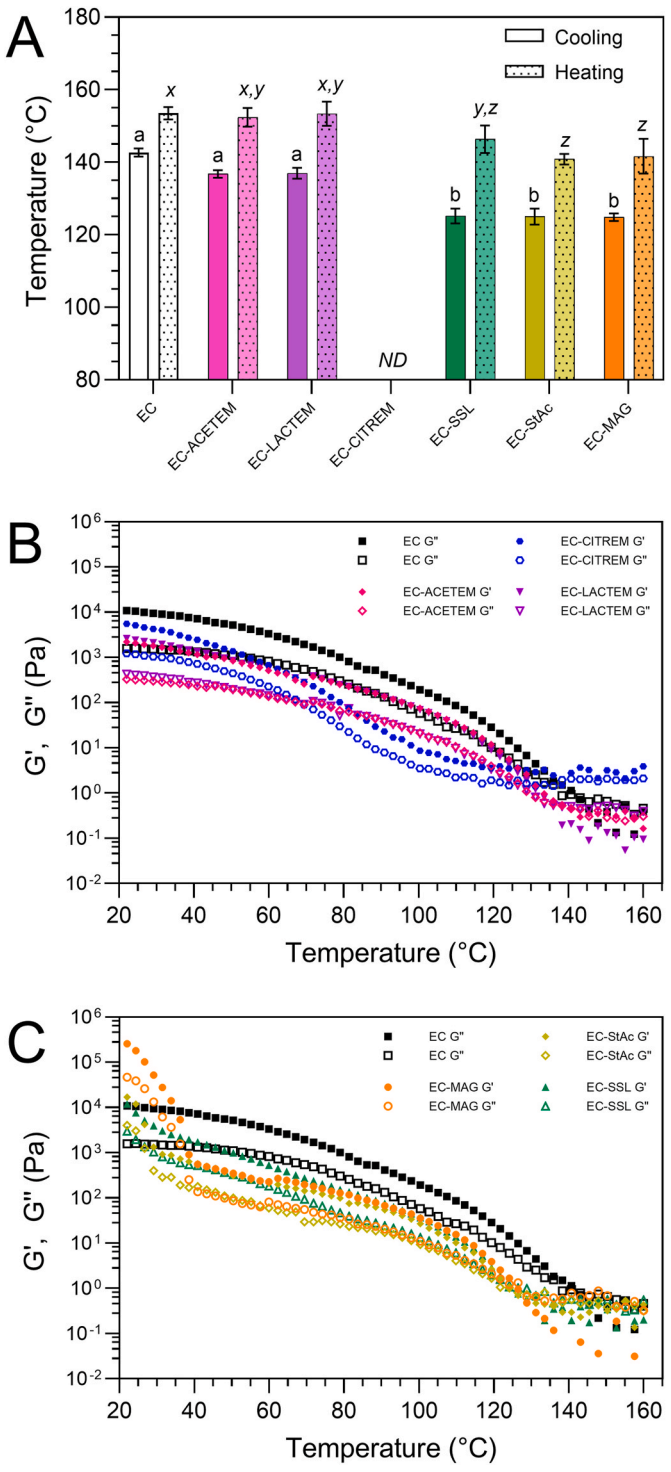

Fig. 7. Thermo-rheological properties of oleogels prepared with 8% EC and 4% various small molecule additives: cross-over temperatures during cooling and heating cycles (A), and temperature sweep profiles during the first cooling cycle (B,C). *For sample nomenclature, the reader is referred to Section 2.1.

the oleogels relative to EC alone, suggesting they had a plasticizing effect on the polymer network (Gravelle et al., 2016). Similar results have been reported for various ASMs, such as sorbitan and glycerol esters of both stearic and oleic acid (Davidovich-Pinhas, Gravelle, et al., 2015), stearic acid/stearyl alcohol mixture (Gravelle, Davidovich-Pinhas, et al., 2017), and lauric acid (Haj Eisa et al., 2020). In contrast, LACTEM an ACETEM did not produce a statistically significant change in the

cross-over temperature. As these ASMs also produced comparatively smaller increases in oleogel mechanical strength (Fig. 3), this further underlining the relatively minor interaction between these molecules and EC.

When cooling from the melt, a two-step increase in G′ was observed in the EC-based oleogels prepared with MAG, StAc, and SSL (Fig. 7C). The first increase in G′ occurred gradually as the temperature was reduced below 140 °C. This is indicative of the formation of EC polymer-polymer junction zones (Davidovich-Pinhas, Gravelle, et al., 2015), and was observed in all samples evaluated. The second, abrupt increase in G′ can be attributed to the formation of ASM crystals, with the increase initiating at 38 °C, 26 °C, and 32 °C for MAG, StAc, and SSL, respectively. These values are slightly lower than those observed by differential scanning calorimetry (Table 2), but follow the same overall trend. A similar increase was not observed for LACTEM due to the lower crystallization temperature (<20 °C). The abrupt decrease in G′ associated with the melting of these crystal networks was also observed, occurring at 56 °C, 50 °C, and 42 °C for MAG, StAc, and SSL, respectively. Finally, although the EC-CITREM oleogels did not display a cross-over, the thermal profiles indicate the formation of the gel network occurred at lower temperatures, beginning in the range of 80–100 °C (Fig. 7B), further indicating the plasticizing effect caused by the carboxylic acid functional groups of this ASM. Full cooling and heating cycles for all samples are provided as supplementary information (Fig. S2).

3.4.3. Thixotropic behavior

The thixotropic properties of the EC-ASM oleogels were measured to evaluate how the various ASMs impacted the polymer network's ability to recover after being subjected to high strain. The thixotropy test of was performed using a five-stage strain protocol cycling between 0.1% and 100% strain (Fig. 8). The first (low strain) stage determines the initial gel properties, after which the application of high strain was used to apply large deformation well beyond the LVE region. Upon returning to a low applied strain, the temporal recovery in G′ was evaluated relative to that observed during the initial stage.

As shown in Table 4, samples with different ASMs showed quite different recovery behavior. It was observed that EC-MAG had the highest storage modules during the initial low-strain stage, followed by EC-StAc. Both these systems had extremely low recovery immediately after completing the first high-strain stage (0.18 % and 0.15 % recovery, respectively), but continued to recover over a much longer timeframe than all other EC-ASM oleogels evaluated. The difference in the recovery

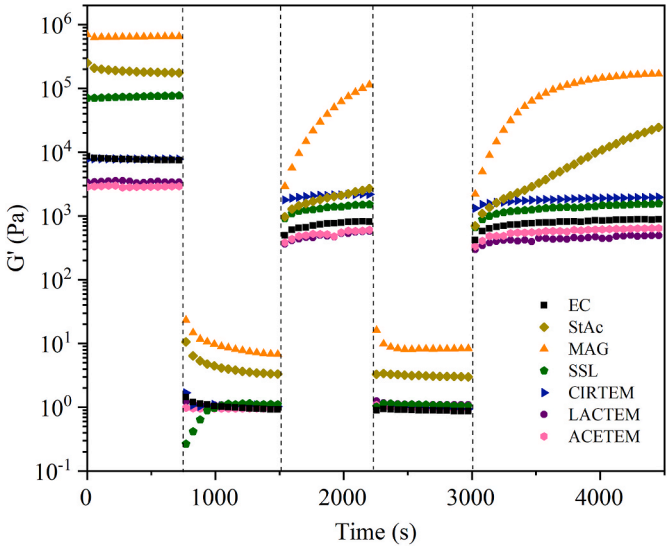

Fig. 8. Thixotropic behavior of EC-based hybrid oleogels with different ASMs. *For sample nomenclature, the reader is referred to Section 2.1.

Table 4
Thixotropic recovery of oleogels prepared with 8 wt% EC or 8% EC and 4 wt% ASMs.

Sample	Recovery (%)
EC	11.7
EC-StAc	26.3
EC-MAG	14.5
EC-SSL	1.8
EC-CITREM	28.5
EC-LACTEM	18.8
EC-ACETEM	22.1

profiles was also likely due to the differences in polymer-crystal interactions, as discussed previously. Similar recovery profiles have also been reported for both MAG alone and EC-MAG oleogels (Rodríguez-Hernández et al., 2021). These profiles indicate reorganization of the crystal network continues over an extended period and may be slowed by the association with the rigid polymer network. The greater degree of recovery provided by StAc may be related to its stronger association with the polymer backbone, whereas MAG crystals were found to extend into the bulk oil phase (see Fig. 3). The EC-SSL oleogels showed very poor recovery (10-fold reduction relative to the EC control), indicating that while the ionic species produced a considerable increase in gel strength and may provide additional support to polymer-polymer junction zones, the dispersed crystallites do not form a system-spanning network, and once damaged, are unable to contribute to the recovery of the polymer network. As noted previously, this is consistent with the relatively low F_b and oil loss observed under large deformations.

All remaining EC-ASM oleogels displayed thixotropic profiles similar to the oleogel structured with EC alone, indicating the overall recovery profile was largely dominated by the polymer network, with the ASMs contributing to the extent of recovery. Similar to StAc, the higher recovery provided by CITREM can be attributed to the strong interaction between EC and the carboxylic acid functional groups. Further, the unsaturated tail groups likely contributed to the more rapid recovery in the thixotropy profile, as compared to the EC-StAc system. Both LACTEM and ACETEM also provided moderate recovery after applying large amplitude shear. As neither of these additives formed crystals at room temperature, they would primarily facilitate favorable interactions between the polymer and oil phase, which has also been shown to improve oil binding and increase elastic behavior (Gravelle et al., 2016). The lower recovery relative to CITREM can thus be attributed to the lower polarity of the functional groups in these ASMs.

3.4.4. Large amplitude oscillatory shear (Laos) tests

Many of the desirable performance characteristics of fats are related to their nonlinear viscoelastic behavior; i.e., that occurring beyond the LVE region (Macias-Rodriguez, Ewoldt, & Marangoni, 2018). For this reason, LAOS measurements were used to evaluate how each of the ASMs impacted the nonlinear response of the EC-ASM oleogels. The full oscillatory response at each imposed intercycle strain (γ_0) was analyzed using elastic Lissajous plots and the results under strains 0.1%, 1.01%, 10%, 101% and 1010% are present in Fig. 9. All elastic Lissajous plots showed a narrow and elliptical shape at the lowest γ_0 (0.101%), which is typical behavior within the LVE region (Ewoldt et al., 2008; John et al., 2019). At $\gamma_0 = 1.01\%$, the elastic Lissajous plots of oleogels structured with EC alone and both the EC-ACETEM and EC-LACTEM oleogels remained quite narrow and nearly elliptical. The other oleogels began to display some evidence of nonlinearity, having a larger enclosed loop area caused by viscous energy dissipation. The EC-MAG (and to a lesser extent, the EC-StAc) oleogels also became somewhat distorted, displaying a moderate upswing in the elastic Lissajous plot, indicative of strain stiffening. This behavior can likely be attributed to strain build-up within the crystal network in response to the applied deformation. A similar intracycle strain stiffening phenomenon has been seen in the

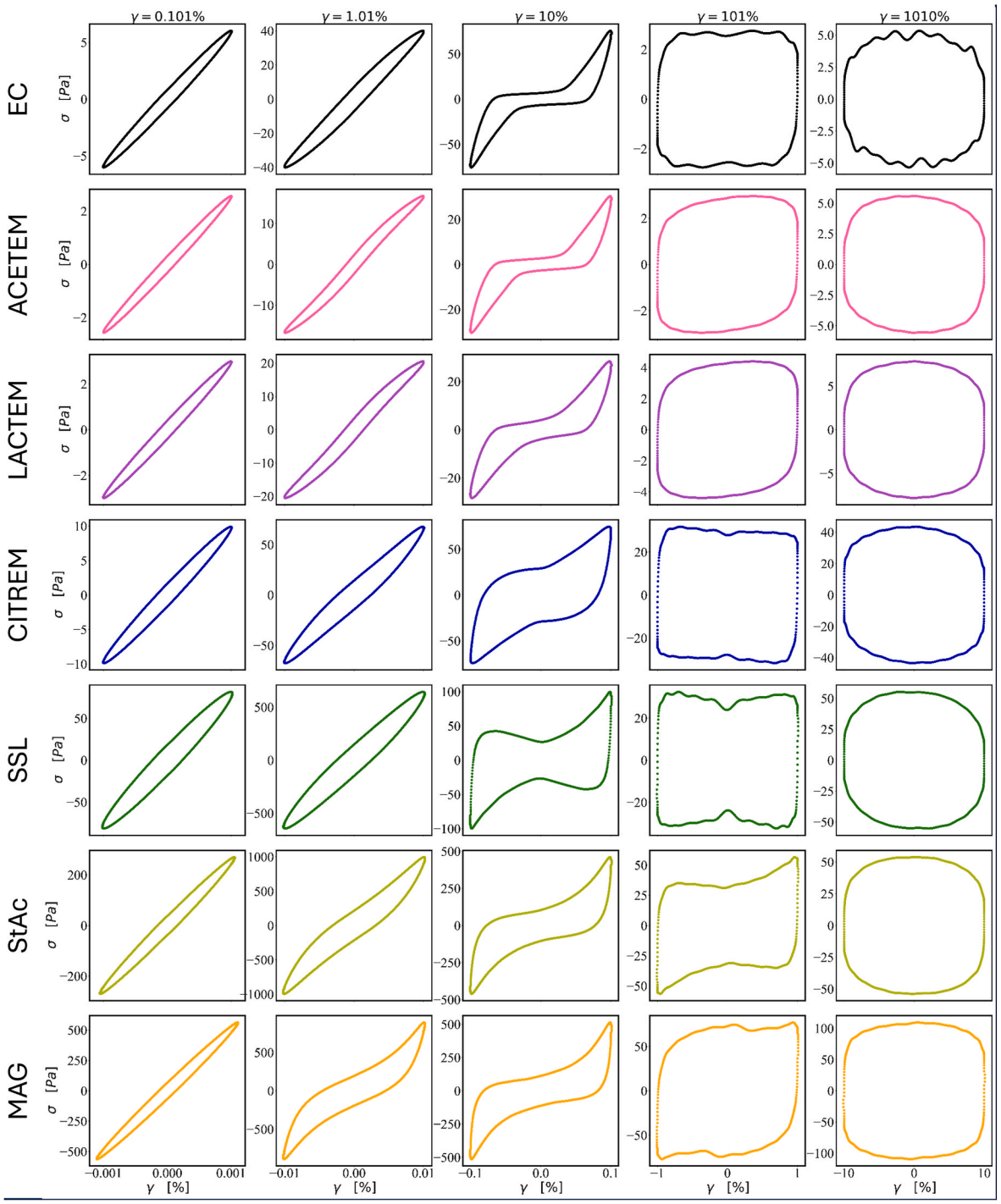

Fig. 9. Elastic Lissajous plots of total stress (σ) vs. strain (γ) for the EC-based oleogel (from top to bottom): EC only, EC-ACETEM, EC-LACTEM, EC-CITREM, EC-SSL, EC-StAc, and EC-MAG with imposed strain (γ_0) of 0.101%, 1.01%, 10%, 101% and 1010%. *For sample nomenclature, the reader is referred to Section 2.1.

LAOS behavior of emulsion gels (Li, Xu, et al., 2021) and biopolymer networks (John et al., 2019). Further, the effect may be more pronounced in the EC-MAG system due to the MAG crystals extending throughout the oil phase to form a system-spanning network (see Fig. 3C).

As the strain increased, the extent of ellipse distortion became more prominent in all samples. At γ_0 = 10.1%, the Lissajous plots of the oleogel structured with EC alone transitioned to a prominent narrow, inverted sigmoidal shape. The pronounced upswing indicates a high degree of strain stiffening, which could be caused by the stretching of the polymer network, which has been observed in both experimental and computational studies (Park, Ahn, & Lee, 2015; Xia et al., 2021). As some bonds have been irreversibly damaged, there is little or no response at small intracycle strains, but a strong elastic response as the intact chains are deformed (Park et al., 2015). Similar Lissajous plots were observed for the EC-ACETEM and EC-LACTEM oleogels, with EC-LACTEM retaining a greater elastic response at intermediate intracycle strains.

The elastic Lissajous plots of the remaining EC-ASM oleogels at γ_0 = 10.1% became more open compared to the gel structured with EC alone, which is indicative of increased energy dissipation within the structural network. Compared to EC alone, the EC-MAG and EC-StAc oleogels

exhibited a greater degree of energy dissipation, which can be correlated to the presence of the system-spanning crystal networks which both reinforce the polymer gel and provide additional structural support through crystal-crystal interactions. The comparison of the enclosed area can be better seen in normalized Lissajous plots, which are provided as supplementary information (see Fig. S3). Similar results were observed for the EC-CITREM and EC-SSL oleogels, in which the enclosed area expanded dramatically (Fig. 9 and supplementary information, Fig. S3). This can be attributed to the fact that although these additives interact strongly with EC, they do not form system-spanning crystal networks. As noted above, the CITREM may have the opportunity to form physical bonds between multiple polymer strands. While this interaction may plasticize the polymer, the additional junction zones may cause a greater degree of drag and associated energy dissipation as the polymer network is deformed. The EC-SSL elastic Lissajous plot at γ_0 = 10.1% also shows a unique behavior amongst the ASMs investigated, with a "bow-tie" shape indicative of intracycle stress overshoot. This behavior has also been observed in debranched waxy rice starch gels, which was attributed to a coupling of the sample elasticity with instrument inertia effects (Precha-Atsawanan, Uttapap, & Sagis, 2018). However, taken together with the unique microstructure and mechanical properties of the EC-SSL oleogels, this behavior may be related to the mechanism by which SSL reinforces the EC network. The interaction with the highly hydrophilic, ionic species in the SSL headgroup may both reinforce and plasticize the polymer-polymer junction zones. Further, the absence of system-spanning crystal-crystal contacts may limit stress translation, resulting in more localized energy dissipation. This would also account for the gradual increase in gel firmness under large deformation and the intracycle stress overshoot (rapid stress dissipation upon strain reversal).

When strain increased to 101%, most of the EC-ASM oleogel Lissajous plots transitioned into a square-like shape, indicative of plastic behavior, and suggesting considerable structural breakdown. Notably, the EC-StAc oleogel retained a more inverted sigmoidal shape and lower energy dissipation (smaller enclosed area) at this strain. This behavior can be attributed to the disordered large crystal aggregates in EC-StAc, which has also been reported in brittle fats (Macias-Rodriguez et al., 2018). At the largest strain of 1010%, all Lissajous plots showed a similar, nearly rectangular shape, indicating the structural breakdown of all oleogels.

The viscous Lissajous plots shown in the supplementary information (normalized: Fig. S3; magnitude: Fig. S4), demonstrate a gradual change in the shape of these curves from elliptical to near S-shaped curves, suggesting a highly nonlinear viscoelastic behavior with strong shear-thinning at high strain rates. With an increased strain from 0.101% to 1.01%, except for EC-MAG, the curves of all the oleogels were only slightly distorted from the initial elliptical shape. In contrast, EC-MAG had transitioned to exhibit a nonlinear viscous behavior. This indicates it has relatively less elastic solid-like response. When the strain increased to 101%, secondary loops were observed in the viscous Lissajous response of EC-CITREM and EC-SSL. This stress overshoot could be caused by microstructural rearrangement occurring under deformation, which is in line with the analysis of elastic Lissajous plots. The results of LAOS confirm that the EC-ASM oleogels with larger, interconnected crystals (EC-MAG, EC-StAc) were less resistant to large amplitude deformations. Consequently, the crystal formation contributed to the plasticity of the oleogel, showing a gradual microstructural change with increasing strain.

The non-linear rheological behavior of the EC-based oleogels was further quantified using the S-factor and T-factor (Fig. 10). Generally, positive S-factors indicate intracycle strain stiffening behavior, while positive T-factors indicate intracycle shear thickening behavior. As shown in Fig. 10A, the S-factor was positive over the entire measured strain range for samples containing MAG, StAc, SSL, and CITREM. Additionally, the S-factors of all these gels initially increase with strain to a peak, after which EC-CITREM and EC-SSL display a continual reduction, while the EC-MAG and EC-StAc oleogels show only a moderate reduction in the S-factor, effectively reaching a plateau. The first increase exhibited by all 4 oleogels can be attributed to intracycle strain stiffening effects, while the plateau effect in the EC-MAG and EC-StAc systems can be attributed to plastic deformation resulting from the system-spanning crystal networks.

The T-factors of all oleogels were negative, reflecting intracycle shear-thickening behavior (Fig. 10B). A more pronounced decrease in T-factors was observed for the oleogel structured with EC alone, indicating a strong intracycle shear-thickening behavior. This suggests that in the absence of any ASMs, the polymer network was less resistant to deformation, and its structure broke down more readily as the strain rate increased. For the oleogel with CITREM, the T-factor was nearly constant (and near zero) up strain rates of ~40–50 %, reflecting its higher resistance to strain, consistent with the more elastic nature of these gels when subjected to large deformations (as noted previously). The EC-StAc and EC-SSL oleogels showed a gradual decrease in the T-factor up to strains of ~50%, followed by an increase at higher strains. The other gels followed a similar pattern, but some variation in this behavior was observed at intermediate strain, suggesting the reduction in T-factor is associated with the structural breakdown of the various gels. Thus, the addition of ASMs could provide a means of modulating both the small- and large amplitude rheological properties of EC-based oleogels.

4. Conclusion

It has been well established that lipid-based amphiphilic small molecules (ASMs) can dramatically impact the performance of EC-based oleogels. Despite this, a comprehensive investigation into the impact of hydrophilic headgroup properties and microstructure was lacking. To

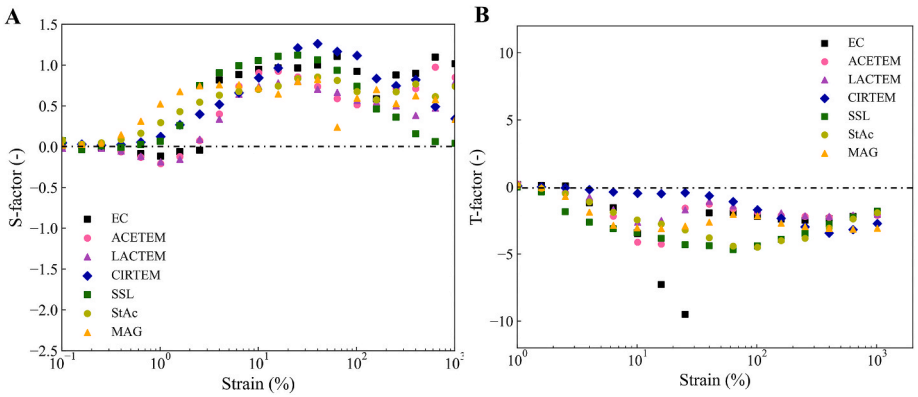

Fig. 10. Ratio of strain stiffening (S-factor; A) and ratio of shear thickening (T-factor; B) for oleogels with different surfactants. *For sample nomenclature, the reader is referred to Section 2.1.

address this knowledge gap, EC-based oleogels were prepared with six food-relevant ASMs, and the microstructural, thermal, mechanical, and rheological properties were evaluated. In the absence of a system-spanning crystal network, the presence of more polar functional groups provided greater impact on gel strength (CITREM > LACTEM > ACETEM). For those ASMs which formed crystals throughout the EC oleogel matrix, crystal morphology was strongly impacted by the EC network, resulting from nucleation along the polymer backbone. The highly polar and charged headgroup of SSL promoted the formation of a homogeneous network of very small crystals which enhanced the strength of the polymer network, but did not improve the interaction with the oil phase. However, the more localized fracture events in the EC-SSL gels favored an increase in toughness over brittleness. This also resulted in a more pronounced stress overshoot when subjected to large amplitude strain. Unsaturated lipid tails or those which did not crystallize at room temperature tended to enhance elasticity. While MAG and StAc produced a similar increase in gel strength, differences in their solubility in the lipid phase arising from the headgroup structure produced dramatically different crystal networks. Despite these differences, both these compounds produced a similar gradual thixotropic recovery and tendency to produce firm and brittle gels. These findings should provide greater insight into the effect different chemical features of lipid-based ASMs will provide in EC-based multi-component oleogels. This in turn could guide appropriate selection of ASMs to develop fat mimetics with optimized performance for a diverse range of food applications.

CRediT authorship contribution statement

Lei Ji: Writing – review & editing, Writing – original draft, Visualization, Methodology, Formal analysis, Data curation. **Andrew J. Gravelle:** Writing – review & editing, Writing – original draft, Visualization, Supervision, Resources, Project administration, Methodology, Investigation, Formal analysis, Data curation, Conceptualization.

Declaration of competing interest

The authors declare that they have no known competing financial interests or personal relationships that could have appeared to influence the work reported in this paper.

Data availability

Data will be made available on request.

Acknowledgements

The authors would like to acknowledge the financial support from the UC Davis Agricultural Experimental Station and the United States Department of Agriculture (USDA) National Institute of Food and Agriculture (NIFA) Hatch/Multi State program.

Appendix A. Supplementary data

Supplementary data to this article can be found online at https://doi.org/10.1016/j.foodhyd.2024.110703.

References

Ahmadi, P., Tabibiazar, M., Roufegarinejad, L., & Babazadeh, A. (2020). Development of behenic acid-ethyl cellulose oleogel stabilized Pickering emulsions as low calorie fat replacer. *International Journal of Biological Macromolecules, 150*, 974–981. https://doi.org/10.1016/j.ijbiomac.2019.10.205

Bascuas, S., Morell, P., Hernando, I., & Quiles, A. (2021). Recent trends in oil structuring using hydrocolloids. *Food Hydrocolloids, 118*, Article 106612. https://doi.org/10.1016/j.foodhyd.2021.106612

Chen, X., Lan, D., Li, D., Wang, W., & Wang, Y. (2024). Enhancement of resistant starch content in ethyl cellulose-based oleogels cakes with the incorporation of glycerol monostearate. *Current Research in Food Science, 8*, Article 100770. https://doi.org/10.1016/j.crfs.2024.100770

Chen, C. H., & Terentjev, E. M. (2009). Aging and metastability of monoglycerides in hydrophobic solutions. *Langmuir, 25*(18), 6717–6724. https://doi.org/10.1021/la9002065

Davidovich-Pinhas, M., Barbut, S., & Marangoni, A. G. (2014). Physical structure and thermal behavior of ethylcellulose. *Cellulose, 21*(5), 3243–3255. https://doi.org/10.1007/s10570-014-0377-1

Davidovich-Pinhas, M., Barbut, S., & Marangoni, A. G. (2015). The role of surfactants on ethylcellulose oleogel structure and mechanical properties. *Carbohydrate Polymers, 127*, 355–362. https://doi.org/10.1016/j.carbpol.2015.03.085

Davidovich-Pinhas, M., Barbut, S., & Marangoni, A. G. (2015). The gelation of oil using ethyl cellulose. *Carbohydrate Polymers, 117*, 869–878. https://doi.org/10.1016/j.carbpol.2014.10.035

Davidovich-Pinhas, M., Gravelle, A. J., Barbut, S., & Marangoni, A. G. (2015). Temperature effects on the gelation of ethylcellulose oleogels. *Food Hydrocolloids, 46*, 76–83. https://doi.org/10.1016/j.foodhyd.2014.12.030

Du, L., & Meng, Z. (2023). Oleofoams and emulsion foams stabilized by sodium stearoyl lactylate: Insight into their relations based on microstructure , rheology and tribology. *Food Hydrocolloids, 137*, Article 108317. https://doi.org/10.1016/j.foodhyd.2022.108317

Ewoldt, R. H., Hosoi, A. E., & McKinley, G. H. (2008). New measures for characterizing nonlinear viscoelasticity in large amplitude oscillatory shear. *Journal of Rheology, 52*(6), 1427–1458. https://doi.org/10.1122/1.2970095

García-Ortega, M. L., Alvarado, M. E. C., Martínez, J. D. P., & Vazquez, J. F. T. (2024). Thermomechanical characterization of oleogels elaborated with a low molecular weight ethyl cellulose and monoglycerides. *Food Biophysics, 1333*. https://doi.org/10.1007/s11483-024-09835-9

García-Ortega, M. L., Toro-Vazquez, J. F., & Ghosh, S. (2021). Development and characterization of structured water-in-oil emulsions with ethyl cellulose oleogels. *Food Research International, 150*, Article 110763. https://doi.org/10.1016/j.foodres.2021.110763

Giacintucci, V., Di Mattia, C. D., Sacchetti, G., Flamminii, F., Gravelle, A. J., Baylis, B., et al. (2018). Ethylcellulose oleogels with extra virgin olive oil: The role of oil minor components on microstructure and mechanical strength. *Food Hydrocolloids, 84*, 508–514. https://doi.org/10.1016/j.foodhyd.2018.05.030

Gravelle, A. J. (2024). Direct oil structuring using ethylcellulose. In C. Palla, & F. Valoppi (Eds.), *Advances in oleogel development, characterization, and nutritional aspects* (pp. 157–175). Cham: Springer. https://doi.org/10.1007/978-3-031-46831-5_7.

Gravelle, A. J., Barbut, S., & Marangoni, A. G. (2012). Ethylcellulose oleogels: Manufacturing considerations and effects of oil oxidation. *Food Research International, 48*(2), 578–583. https://doi.org/10.1016/j.foodres.2012.05.020

Gravelle, A. J., Barbut, S., Quinton, M., & Marangoni, A. G. (2014). Towards the development of a predictive model of the formulation-dependent mechanical behaviour of edible oil-based ethylcellulose oleogels. *Journal of Food Engineering, 143*, 114–122. https://doi.org/10.1016/j.jfoodeng.2014.06.036

Gravelle, A. J., Blach, C., Weiss, J., Barbut, S., & Marangoni, A. G. (2017). Structure and properties of an ethylcellulose and stearyl alcohol/stearic acid (EC/SO:SA) hybrid oleogelator system. *European Journal of Lipid Science and Technology, 119*(11), Article 1700069. https://doi.org/10.1002/ejlt.201700069

Gravelle, A. J., Bovi Karatay, G. G., & Hubinger, M. D. (2024). Oleogels produced by indirect methods. In C. Palla, & F. Valoppi (Eds.), *Advances in oleogel development, characterization, and nutritional aspects* (pp. 231–269). Cham: Springer. https://doi.org/10.1007/978-3-031-46831-5_10.

Gravelle, A. J., Davidovich-Pinhas, M., Barbut, S., & Marangoni, A. G. (2017). Influencing the crystallization behavior of binary mixtures of stearyl alcohol and stearic acid (SOSA) using ethylcellulose. *Food Research International, 91*, 1–10. https://doi.org/10.1016/j.foodres.2016.11.024

Gravelle, A. J., Davidovich-Pinhas, M., Zetzl, A. K., Barbut, S., & Marangoni, A. G. (2016). Influence of solvent quality on the mechanical strength of ethylcellulose oleogels. *Carbohydrate Polymers, 135*, 169–179. https://doi.org/10.1016/j.carbpol.2015.08.050

Haj Eisa, A., Laufer, S., Rosen-Kligvasser, J., & Davidovich-Pinhas, M. (2020). Stabilization of ethyl-cellulose oleogel network using lauric acid. *European Journal of Lipid Science and Technology, 122*(2), 1–10. https://doi.org/10.1002/ejlt.201900044

Hondoh, H., Ueno, S., & Sato, K. (2018). Fundamental aspects of crystallization of lipids. In K. Sato (Ed.), *Crystallization of lipids: Fundamentals and applications in food, cosmetics, and pharmaceuticals* (pp. 105–141). John Wiley & Sons Ltd. https://doi.org/10.1002/9781118593882.ch4.

Hyun, K., Kim, S. H., Ahn, K. H., & Lee, S. J. (2002). Large amplitude oscillatory shear as a way to classify the complex fluids. *Journal of Non-newtonian Fluid Mechanics, 107*, 51–65.

John, J., Ray, D., Aswal, V. K., Deshpande, A. P., & Varughese, S. (2019). Dissipation and strain-stiffening behavior of pectin-Ca gels under Laos. *Soft Matter, 15*(34), 6852–6866. https://doi.org/10.1039/c9sm00709a

Lai, H. L., Pitt, K., & Craig, D. Q. M. (2010). Characterisation of the thermal properties of ethylcellulose using differential scanning and quasi-isothermal calorimetric approaches. *International Journal of Pharmaceuticals, 386*, 178–184. https://doi.org/10.1016/j.ijpharm.2009.11.013

Laredo, T., Barbut, S., & Marangoni, A. G. (2011). Molecular interactions of polymer oleogelation. *Soft Matter, 7*(6), 2734–2743. https://doi.org/10.1039/c0sm00885k

Li, J., Guo, R., Bi, Y., Zhang, H., & Xu, X. (2021). Comprehensive evaluation of saturated monoglycerides for the forming of oleogels. *LWT, 151*(May), Article 112061. https://doi.org/10.1016/j.lwt.2021.112061

Li, Q., Xu, M., Xie, J., Su, E., Wan, Z., Sagis, L. M. C., et al. (2021). Large amplitude oscillatory shear (Laos) for nonlinear rheological behavior of heterogeneous

emulsion gels made from natural supramolecular gelators. *Food Research International, 140*, Article 110076. https://doi.org/10.1016/j.foodres.2020.110076
Lin, Y., Asante, F. O., Xu, X., Li, S., Ding, H., Xu, L., et al. (2021). A naturally tailored small molecule for the preparation of ethyl cellulose supramolecular composite film. *Cellulose, 28*(1), 289–300. https://doi.org/10.1007/s10570-020-03532-9
Lin, Y., Li, M., Xia, J., Ding, H., Xu, L., Yang, X., et al. (2021). Synthesis of plant oil derived polyols and their effects on the properties of prepared ethyl cellulose composite films. *Cellulose, 28*(7), 4211–4222. https://doi.org/10.1007/s10570-021-03811-z
Macias-Rodriguez, B. A., Ewoldt, R. H., & Marangoni, A. G. (2018). Nonlinear viscoelasticity of fat crystal networks. *Rheologica Acta, 57*(3), 251–266. https://doi.org/10.1007/s00397-018-1072-1
Marangoni, A. G. (2017). Steady-state nucleation kinetics: The Fisher turnbull model. In *Kinetic analysis of food systems* (pp. 135–144). Cham: Springer. https://doi.org/10.1007/978-3-319-51292-1.
Meng, Z., Guo, Y., Wang, Y., & Liu, Y. (2019). Oleogels from sodium stearoyl lactylate-based lamellar crystals: Structural characterization and bread application. *Food Chemistry, 292*, 134–142. https://doi.org/10.1016/j.foodchem.2018.11.042
Park, J. D., Ahn, K. H., & Lee, S. J. (2015). Structural change and dynamics of colloidal gels under oscillatory shear flow. *Soft Matter, 11*(48), 9262–9272. https://doi.org/10.1039/c5sm01651g
Pehlivanoğlu, H., Demirci, M., Toker, O. S., Konar, N., Karasu, S., & Sagdic, O. (2018). Oleogels, a promising structured oil for decreasing saturated fatty acid concentrations: Production and food-based applications. *Critical Reviews in Food Science and Nutrition, 58*(8), 1330–1341. https://doi.org/10.1080/10408398.2016.1256866
Pinto, T. C., Sabet, S., Kazerani García, A., Kirjoranta, S., & Valoppi, F. (2024). Oleogel preparation methods and classification. In C. Palla, & F. Valoppi (Eds.), *Advances in oleogel development, characterization, and nutritional aspects* (pp. 77–114). Cham: Springer. https://doi.org/10.1007/978-3-031-46831-5_4.
Precha-Atsawanan, S., Uttapap, D., & Sagis, L. M. C. (2018). Linear and nonlinear rheological behavior of native and debranched waxy rice starch gels. *Food Hydrocolloids, 85*, 1–9. https://doi.org/10.1016/j.foodhyd.2018.06.050
Rodríguez-Hernández, A. K., Pérez-Martínez, J. D., Gallegos-Infante, J. A., Toro-Vazquez, J. F., & Ornelas-Paz, J. J. (2021). Rheological properties of ethyl cellulose-monoglyceride-candelilla wax oleogel vis-a-vis edible shortenings. *Carbohydrate Polymers, 252*, Article 117171. https://doi.org/10.1016/j.carbpol.2020.117171
Rosen-Kligvasser, J., & Davidovich-Pinhas, M. (2021). The role of hydrogen bonds in TAG derivative-based oleogel structure and properties. *Food Chemistry, 334*, Article 127585. https://doi.org/10.1016/j.foodchem.2020.127585
Sabet, S., Pinto, T. C., Kirjoranta, S. J., Garcia, A. K., & Valoppi, F. (2023). Clustering of oleogel production methods reveals pitfalls and advantages for sustainable, upscalable, and oxidative stable oleogels. *Journal of Food Engineering, 357*, Article 111659. https://doi.org/10.1016/j.jfoodeng.2023.111659
Sagiri, S. S., Singh, V. K., Pal, K., Banerjee, I., & Basak, P. (2015). Stearic acid based oleogels: A study on the molecular, thermal and mechanical properties. *Materials Science and Engineering: C, 48*, 688–699. https://doi.org/10.1016/j.msec.2014.12.018
Shakeel, A., Farooq, U., Gabriele, D., Marangoni, A. G., & Lupi, F. R. (2021). Bigels and multi-component organogels: An overview from rheological perspective. *Food Hydrocolloids, 111*(July 2020), Article 106190. https://doi.org/10.1016/j.foodhyd.2020.106190
Shlush, E., & Davidovich-Pinhas, M. (2023). Fabrication of bioplastic material based on ethyl-cellulose using hot-melt extrusion. *Food Packaging and Shelf Life, 40*, Article 101206. https://doi.org/10.1016/j.fpsl.2023.101206
Silva, S. S., Rodrigues, C., Fernandes, E. M., Lobo, C. M., Gomes, J. M., & Reis, R. L. (2022). Tailoring natural-based oleogels combining ethylcellulose and virgin coconut oil. *Polymers, 14*, 2473.
Sivakanthan, S., Fawzia, S., Madhujith, T., & Karim, A. (2022). Synergistic effects of oleogelators in tailoring the properties of oleogels: A review. *Comprehensive Reviews in Food Science and Food Safety*, 1–32. https://doi.org/10.1111/1541-4337.12966
Soleimanian, Y., Ghazani, S. M., & Marangoni, A. G. (2024a). Ethylcellulose oleogels of oil glycerolysis products as functional adipose tissue mimetics. *Food Hydrocolloids, 151*, Article 109756. https://doi.org/10.1016/j.foodhyd.2024.109756
Soleimanian, Y., Ghazani, S. M., & Marangoni, A. G. (2024b). Rheological properties of ethylcellulose oleogels of oil glycerolysis products as functional adipose tissue mimetics. *Food Hydrocolloids, 151*, Article 109868. https://doi.org/10.1016/j.foodhyd.2024.109868
Valoppi, F., Calligaris, S., Barba, L., Segatin, N., Ulrih, N. P., & Nicoli, M. C. (2017). Influence of oil type on formation, structure, thermal, and physical properties of monoglyceride-based organogel. *European Journal of Lipid Science and Technology, 1500549*, 1–10. https://doi.org/10.1002/ejlt.201500549
Vélez-Erazo, E. M., Okuro, P. K., Gallegos-Soto, A., da Cunha, R. L., & Hubinger, M. D. (2022). Protein-based strategies for fat replacement: Approaching different protein colloidal types, structured systems and food applications. *Food Research International, 156*, Article 111346. https://doi.org/10.1016/j.foodres.2022.111346
Vereecken, J., Meeussen, W., Foubert, I., Lesaffer, A., Wouters, J., & Dewettinck, K. (2009). Comparing the crystallization and polymorphic behaviour of saturated and unsaturated monoglycerides. *Food Research International, 42*(10), 1415–1425. https://doi.org/10.1016/j.foodres.2009.07.006
Wang, Z., Chandrapala, J., Truong, T., & Farahnaky, A. (2023). Multicomponent oleogels prepared with high- and low-molecular-weight oleogelators: Ethylcellulose and waxes. *Foods, 12*, 3093. https://doi.org/10.3390/foods12163093
Xia, W., Siu, W. K., & Sagis, L. M. C. (2021). Linear and non-linear rheology of heat-set soy protein gels: Effects of selective proteolysis of β-conglycinin and glycinin. *Food Hydrocolloids, 120*, Article 106962. https://doi.org/10.1016/j.foodhyd.2021.106962
Zetzl, A. K., Gravelle, A. J., Kurylowicz, M., Dutcher, J., Barbut, S., & Marangoni, A. G. (2014). Microstructure of ethylcellulose oleogels and its relationship to mechanical properties. *Food Structure, 2*(1–2), 27–40. https://doi.org/10.1016/j.foostr.2014.07.002
Zhang, Y., Zhang, R., Ying, J., Li, S., Gao, Y., & Mao, L. (2024). Tailoring microstructures of oleogel-based HIPEs to modulate oral processing properties: Rheology, tribology and mastication effects. *Food Hydrocolloids, 153*, Article 109968. https://doi.org/10.1016/j.foodhyd.2024.109968
Zhang, R., Zhang, Y., Yu, J., Gao, Y., & Mao, L. (2022). Rheology and tribology of ethylcellulose-based oleogels and W/O emulsions as fat substitutes : Role of glycerol monostearate. *Foods, 11*(15), 2364. https://doi.org/10.3390/foods11152364